

DesignCon 2010

Impact of Copper Surface Texture on Loss: A Model that Works

Paul G. Huray, University of South Carolina,
huray@sc.edu

Olufemi(Femi) Oluwafemi, Intel Corporation,
olufemi.b.oluwafemi@intel.com

Jeff Loyer, Intel Corporation,
jeff.loyer@intel.com

Eric Bogatin, Bogatin Enterprises,
eric@BeTheSignal.com

Xiaoning Ye, Intel Corporation,
xiaoning.ye@intel.com

Abstract

Surface roughness of copper can more than double conductor power losses in high speed serial interconnects. Empirical models of copper roughness are not accurate enough for data rates > 5 Gbps to ensure signal integrity. An electromagnetic model has been developed using a rigorous application of Maxwell's equations, based on observed copper surface texture. This model accurately describes attenuation and dispersion of signals, and its correlation has been confirmed through simulations and measurements up to 50 GHz. One conclusion of this model is that the conventional description of RMS surface roughness is misleading, yielding inaccurate predictions and misinterpretations of how currents flow on interconnects.

Author's Biography

Dr. Paul Huray is Professor of Electrical Engineering at the University of South Carolina. Huray has worked at the Oak Ridge National Laboratory, Intel, and the White House. Huray introduced the first graduate program on signal integrity and is the author of *Maxwell's Equations* and *The Foundations of Signal Integrity*.

Dr.Olufemi(Femi) Oluwafemi obtained a BS degree in Physics from Obafemi Awolowo University, Nigeria, an M.S. degree in Applied Physics, from Pittsburg State University, Kansas, and a Ph.D. degree in electrical engineering from the University of South Carolina. He is a Signal Integrity lead for the Visual Computing Group at Intel.

Jeff Loyer is a Signal Integrity Lead for Intel's Enterprise Server Division. He has authored articles on signal integrity for DesignCon, EDN and Printed Circuit Design & Manufacture. He holds a BS degree in electrical-engineering technology from Arizona State University (Tempe), and has taught signal-integrity classes inside and outside Intel.

Dr. Eric Bogatin is Signal Integrity Evangelist with Bogatin Enterprises, a leader in signal integrity training. He received a BS in physics from MIT and an MS and PhD in physics from the University of Arizona. He held senior engineering and management positions at Bell Labs, Raychem and Sun Microsystems.

Dr. Xiaoning Ye is a senior hardware engineer with Intel, responsible for high speed design guidelines in Server Platforms. He received BS and MS degrees from Tsinghua University, China and a PhD in electrical engineering from University of Missouri – Rolla. He has authored 30 IEEE papers and holds 6 patents.

Background: In 1949 Samuel Morganⁱ published the first study on conductor surface roughness losses using a numerical solution to 1% accuracy for Maxwell's equations using a 2-D surface

distortion model. He determined that, at 10 GHz, current flow transverse to periodic structures could increase loss by up to 100%! If the current flow was parallel, the losses increased by up to 33%. Morgan hypothesized the cause for this additional loss was based on the assumption that the loss was a function of the RMS distortion of a rough surface relative to the electromagnetic skin depth, δ , of a perfectly smooth metal surface with conductivity equal to that of the bulk metal. He studied two-dimensional cases that assumed the roughness consisted of infinitely long grooves parallel or normal to the current flow. Three geometrical shapes studied by Morgan were square, rectangular, and equilateral triangle grooves. The power loss of the rough surface, P_{rough} , relative to that of a smooth surface, P_{smooth} is shown plotted in figure 1 as a function of RMS deviation / Skin Depth (Δ/δ). The Morgan analysis was conducted before the advent of computers so we must be in awe of a researcher who, with his “computer” (Miss J. G. Asbury - who performed the calculations by hand) would persist to numerically calculate a solution to Maxwell’s equations to 1% precision.

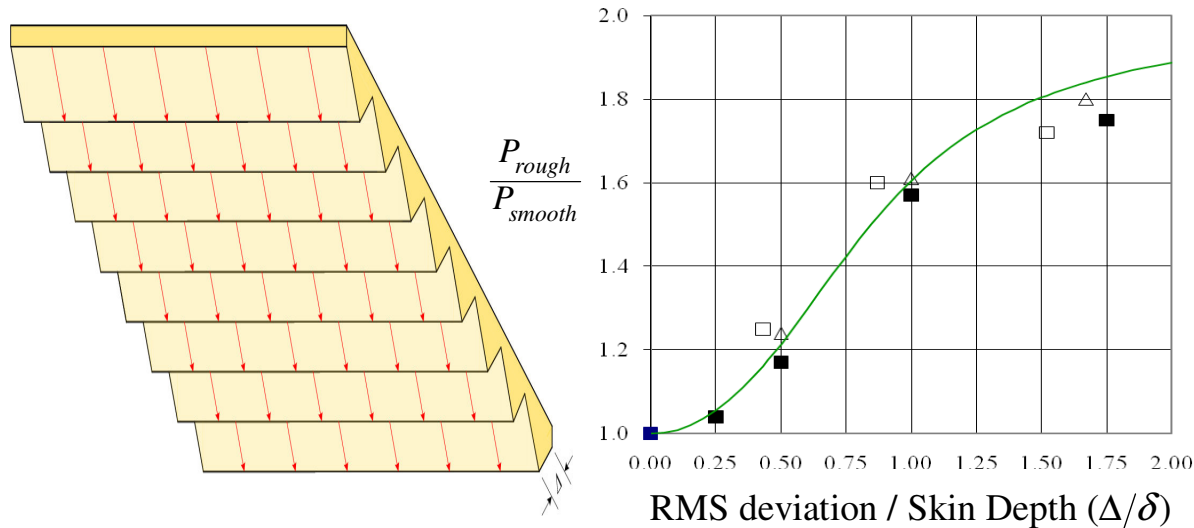


Figure 1. Samuel Morgan’s 2-D relative power loss calculations for rectangular (□), triangular (Δ), and square (■) grooves that are normal to the direction of current flow in a transmission line. Morgan’s equilateral triangular distortion perpendicular to the direction of current flow (arrows) is shown in the graphic on the left.

Superimposed on the Morgan data is an empirical fit (solid line) of an arctangent function that Hammerstad postulatedⁱⁱ in 1975 and publishedⁱⁱⁱ in 1980.

$$\frac{P_{rough}}{P_{smooth}} = 1 + \frac{2}{\pi} \arctan \left[1.4 \left(\frac{\Delta}{\delta} \right)^2 \right] \quad (1)$$

The Hammerstad empirical fit to the Morgan data ignored the losses due to parallel grooves and the inverse tangent function had no physical basis. The empirical function (1) is seen to produce a maximum value of 2 for the ratio of rough to smooth power loss.

It is surprising that data obtained by a numerical solution (before the age of digital computers) to a 2-D quasi-static form of Maxwell's equations and an empirical fit to that data is still the basis of surface roughness power losses in some numerical field solvers. It is even more surprising, given that the empirical fit given by equation (1), in association with an analysis of the losses caused by the dielectric propagating medium, falls far short of the insertion loss measured^{iv} by a vector network analyzer (VNA) at frequencies above 5 GHz for microstrip or striplines in many different materials (FR-4, Isola, Rogers, Nelco).

The absorption by fields propagating in a dielectric material has been studied by this group and reported in various presentations and publications^{v,vi,vii}. We have shown that absorption by the propagating medium ("dielectric loss") accounts for about half of the loss; i.e. the total power loss for a 7 inch high-profile trace on a composite *low-loss resin* with a glass fiber weave microstrip is only 18 dB at 50 GHz (the total power loss for a 7 inch low-profile trace on a composite *low-loss resin* is only 15 dB). Figure 2 shows the measured insertion loss (blue curve) for a 7 inch long high profile surface texture microstrip with an *FR-4* propagating medium^{viii}.

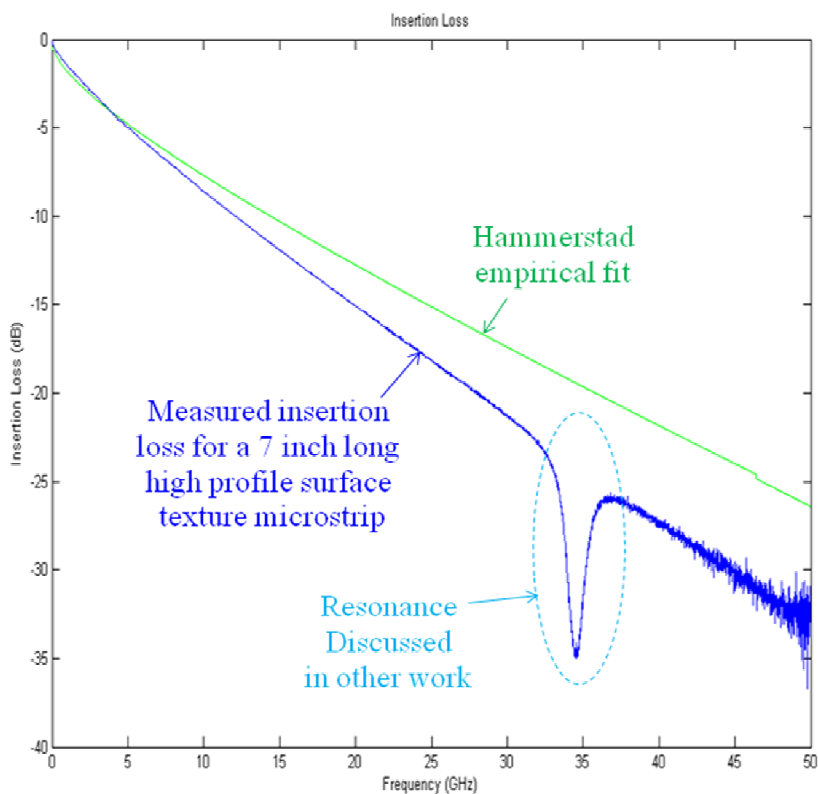


Figure 2. The measured insertion loss data for an isolated 7 inch long transmission line with an FR-4 propagating medium is shown in blue plotted as a function of frequency between 1-50 GHz. The solid green curve (above the data) is a fit of the Djordjevic model for FR-4 dielectric losses combined with the Hammerstad empirical fit surface roughness loss of equation 1.

In figure 2 it is seen that the measured data is approximately in agreement with the Djordjevic dielectric loss and Hammerstad rough surface empirical fit loss only in the regime between 0 and 5 GHz. For frequencies above 10 GHz the inconsistency between the measured data and the Hammerstad empirical fit is unacceptably large. The absorption peak at about 35 GHz is discussed in other publications^{viii}.

Misunderstanding of Current flow and Power Loss: Graphics like figure 1 can lead to a misunderstanding of surface **current** flow at the conductor / dielectric interface for a transmission line. For example, we show a signal pulse in profile as it propagates down a transmission line with an equilateral triangle surface distortion in figure 3. In all of the following graphs, a color convention of red is used for **scalar potential**, **charge**, **charge density**, and **electric field intensity** while blue is used for **current**, **current density**, and **magnetic field intensity**.

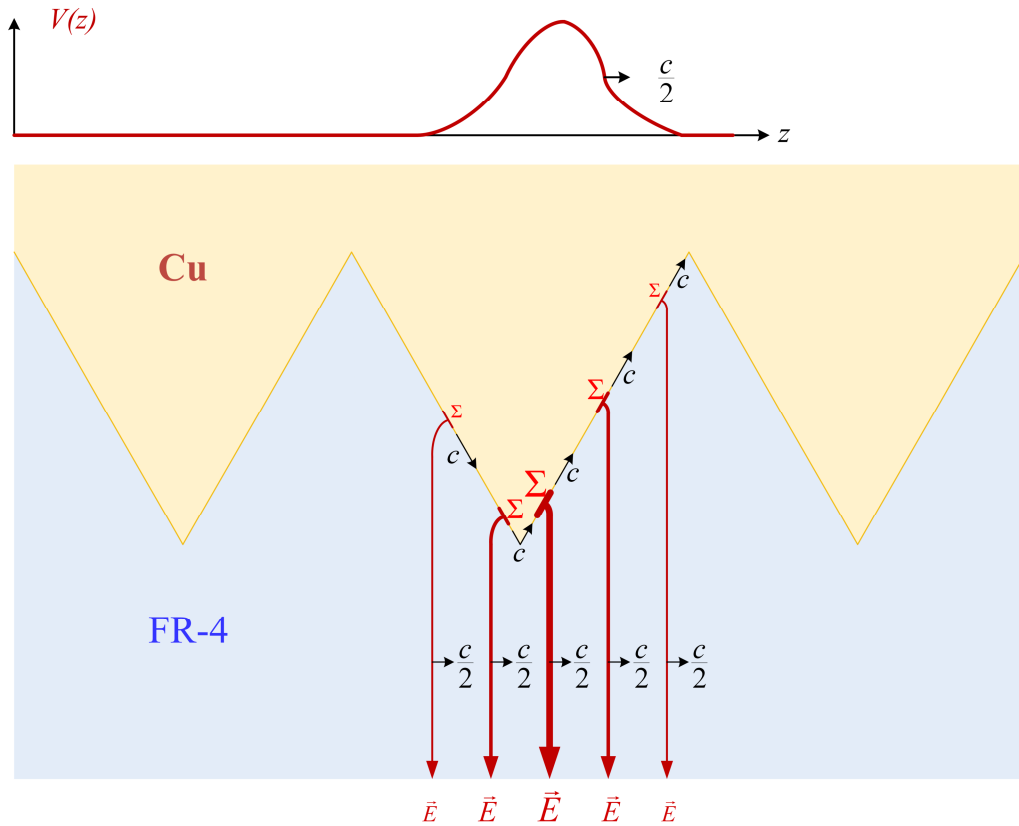


Figure 3. Snapshot of a signal **voltage** pulse (and corresponding **electric field intensity**) as it propagates in a transmission line with an equilateral triangle tooth structure.

The propagation of **electric field intensity**, $\vec{E} = \hat{a}_x E_0$, at a phase velocity of $\vec{u}_p = \hat{a}_z c / \sqrt{\epsilon_r}$ along the transmission line (in the z -direction) requires a surface **charge density**, Σ , on the copper surface to satisfy Gauss's Law. Since the local **electric field intensity** near a copper surface must be normal to the surface, the surface **charge density** on the equilateral triangle tooth must move

along the conductor profile at a speed c if the electric field intensity propagates in the FR-4 at speed $c/2$ for a relative permittivity of $\epsilon_r=4$. Note that for a lower relative permittivity or a steeper conductor profile the surface **charge density** speed exceeds c . Because the fastest conduction electron is at the copper Fermi velocity, $v_F \approx 1.5 \times 10^6 \text{ m/s}$, one must ask, “How is the surface **charge density** velocity supported by local **charge** rearrangement?”, “Does one need to take into account space contraction for the propagating **charge**?”, “Can surface **charge density** propagate along a conductor at a speed that exceeds c ? ” and “If the **current** is travelling a longer path on a transmission line, why is the time of arrival not substantially lengthened for rough vs. flat surfaces?” The answer is that local surface **charge density** is formed by the displacement of conduction electrons transverse to the surface profile so that a *wave of charge density* propagates at whatever speed is needed to support the external **electric field intensity** in the transmission line. No charged particles actually move at relativistic speeds so we need not take into account space contraction.

Some incorrect interpretations even suggest there is an exponentially declining **current density** profile moving along a flat conductor surface as shown in figure 4.

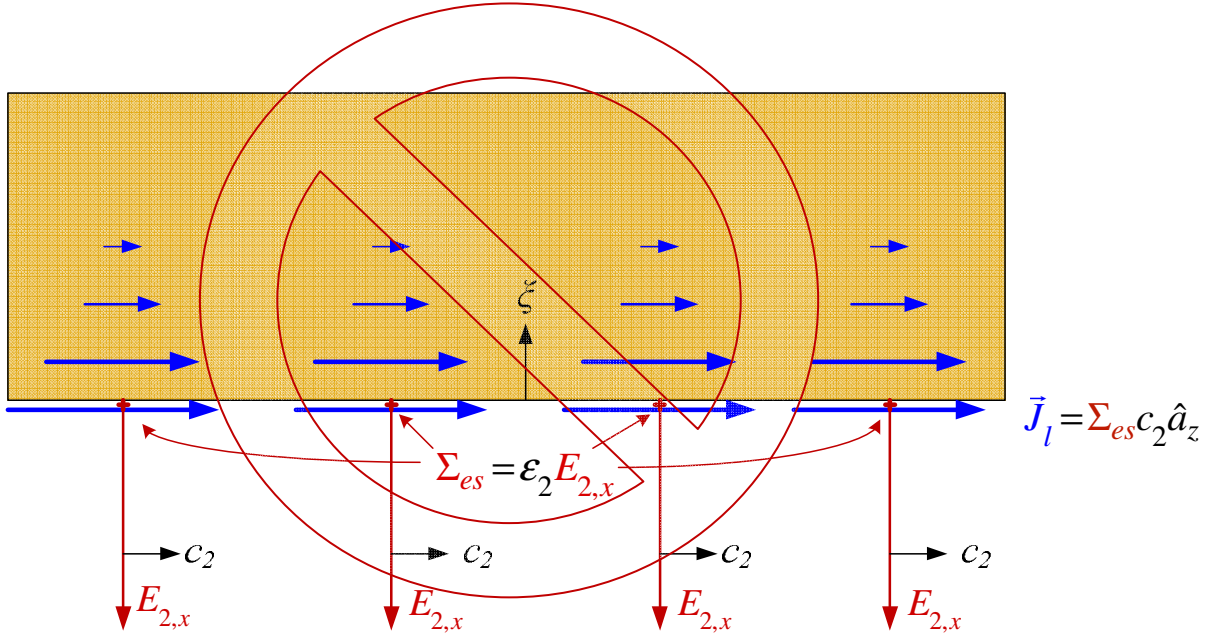


Figure 4. Snapshot of a propagating signal **electric field intensity** and the incorrect model of surface **current density**, J_l , as it propagates inside a perfectly flat transmission line.

The **current density** shown in figure 4 is often described as exponentially decreasing with the variable ξ as one proceeds into the conductor. A few models even integrate the **current density** between $\xi=0$ to $\xi=\infty$ to show that a constant surface **current** to a depth of $1/\delta$ gives the same total conductor **current** with a conclusion that, “it is a valid approximation to assume that all the

current is flowing in an area confined by the conductor width and a single skin depth.” Unfortunately, this incorrect model results in a current loss analysis like that shown in figure 5.

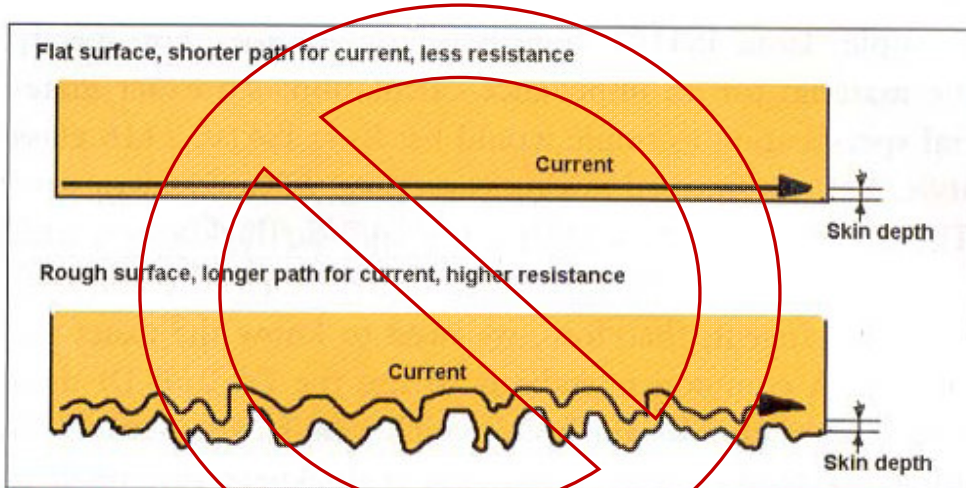


FIGURE 7. How roughness increases length and resistance.

Figure 5. Example of an incorrect interpretation of the current path for a rough surface.

By incorrectly viewing the current density profile into the good conductor by a distance, ξ , as an exponentially decaying current distribution and using an analysis that this current profile follows the surface features to produce an ohmic loss as it interacts with surface resistance leads to several illogical conclusions. We must ask, “How does current density instantaneously appear as an exponentially decreasing function?” “Have we suspended causality that requires a source and a time retarded response at distance ξ ?” “How does the current density flow around protrusions that are infinitely steep or double back?” “Would an isolated conducting material have no influence on power loss?” We conclude that neither the exponential current penetration nor the ohmic loss concept is correct!

Field Propagation Concept: As explained^{viii} in *The Foundations of Signal Integrity*, and shown in figure 6, the normal component of the local electric field intensity, \vec{E}_\perp , does not penetrate a perfect electric conductor due to a surface charge density required by Gauss’s law but falls immediately to zero at the surface as would occur in a static field model. Because the conduction electrons in a *good* conductor like copper can move at velocities sufficient to null free charges with a lifetime of 10^{-19} seconds, we can also say that copper *quasi-statically* nulls the normal component of the electric field intensity for frequencies below 10^{15} Hz. The results of electromagnetic field penetration from a propagating medium like FR-4 into an adjacent *good* conductor behaves as shown in figure 6.

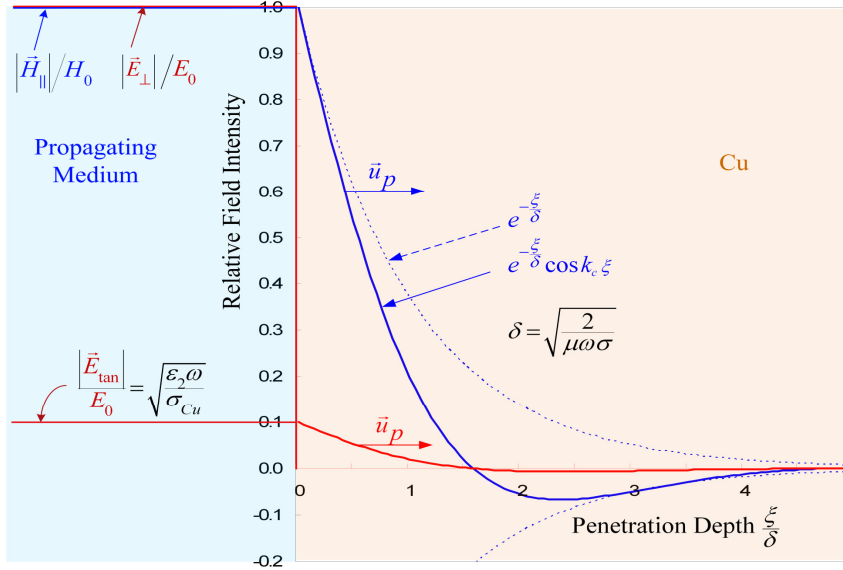


Figure 6. Relative tangential **magnetic** and normal **electric** field intensity in the propagating medium (upper left) adjacent to a perfectly flat copper transmission line and the relative fraction of each that penetrates into the conductor. Inside the copper is the cosinusoidally modulated exponential decay for a harmonic applied **magnetic field intensity** (solid line) and the induced **tangential electric field intensity** (that leads \vec{H}_{\perp} in the conductor by 45°).

The tangential **electric field intensity** at the conductor surface subsequently is continuous across the dielectric interface and induces a tangential **electric field intensity**, \vec{E}_{\tan} , back into the propagating medium as is shown in the lower left. By contrast the local **magnetic field intensity**, \vec{H}_{\perp} , is tangent to and is continuous across the conductor surface with an exponentially decreasing magnitude as shown in figure 6. It is important to note by the vector, \vec{u}_p , the **magnetic field intensity** propagates normally into a copper conductor at phase velocity

$$\vec{u}_p = \omega \delta \hat{a}_\xi = \frac{c}{\sqrt{\sigma_{Cu}/2\omega\epsilon_0}} \hat{a}_\xi = \begin{bmatrix} c/22,804 & \text{at} & 1 \text{ GHz} \\ c/7,211 & \text{at} & 10 \text{ GHz} \\ c/2,280 & \text{at} & 100 \text{ GHz} \end{bmatrix} \hat{a}_\xi \quad (2)$$

which is *much* slower than the speed of propagation in the propagating medium even at high frequencies. Thus, by the time the **magnetic field intensity** has propagated a distance, ξ , into the copper conductor the inducing external **magnetic field intensity** in the propagating medium (travelling at speed $c/2$) has moved 1,140 times that distance along the transmission line even at a frequency of 100 GHz. We can also see that for a harmonic inducing **magnetic field intensity** the penetrating field will vary co-sinusoidally and change sign as it penetrates distance ξ into the

copper; the solid blue line shows negative penetrating fields beyond $\xi/\delta = \pi/2$ that were induced from an earlier time. Maxwell's equations require an accompanying tangential electric field intensity inside the copper conductor that propagates with the same phase velocity, $u_p = u_p$, but which leads the magnetic field intensity by 45° . This is shown by the lower solid red curve in the Cu region; note the magnitude of the electric field intensity curve relative to the magnetic field intensity curve is frequency dependent and, in this case, is exaggerated to show the penetrating behavior. Finally we note that a boundary condition for tangential electric field intensity inside the conductor must be continuous across the dielectric boundary so that an additional electric field intensity, $\bar{E}_{\tan} = \hat{a}_z |\bar{E}_0| / \sqrt{\sigma_{Cu}/\omega\epsilon_2}$, appears in the dielectric due to the surface conductivity of the copper; the magnitude of this field is *much* smaller than the original inducing field, $|\bar{E}_0|$ and is out of phase with it by 45° . The ratio $|\bar{E}_{\tan}| / |\bar{H}_0|$ is called the surface impedance (which we will use later) and depends on the square root of frequency. This field also destroys the TEM nature of the propagating electromagnetic waves in the dielectric medium.

Time Retarded fields and current densities in copper: Because a signal electric field intensity propagates at $c_2 = c/\sqrt{\epsilon_r}$ in the medium, it requires a surface charge density, Σ_{es} , on the adjacent conductor that must move with the electric field intensity in the z -direction at the same speed, c_2 . This moving surface charge density is a wave formed by the transverse displacement of the copper conduction electrons and the motion of the surface charge density constitutes a linear surface current density propagating in the z -direction as shown in figure 7.

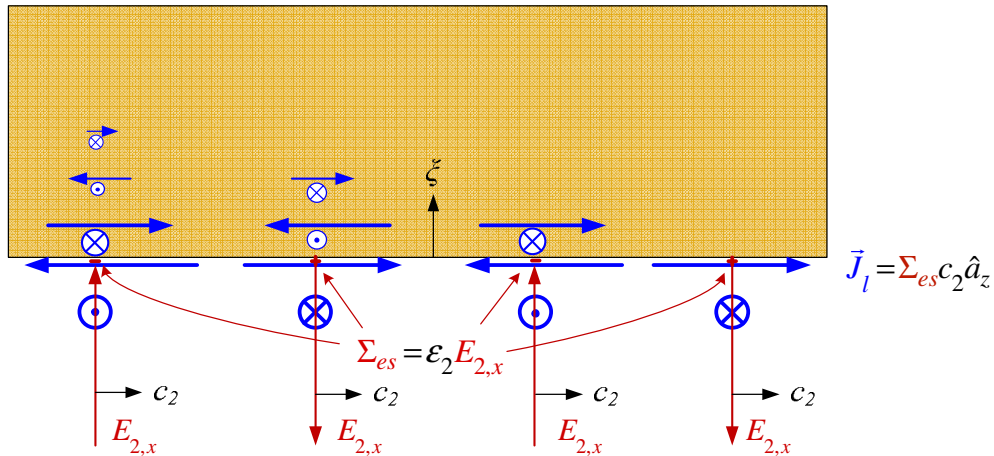


Figure 7. Snapshot of a harmonic electric and magnetic field intensity as it propagates in a medium and the penetration of the tangential magnetic component into the adjacent conductor.

Shown on this graphic is the surface current density (just below the copper) and the induced magnetic field intensity that propagates slowly and decays exponentially into the conductor as

shown in figure 6. Also shown in figure 7 is the consequential **eddy current** that occurs due to the **electric field intensity** internal to the conductor. Note that the induced **current density** in the conductor lags the **surface current density** at the signal wavefront due to the relatively slow propagation of fields into the conductor. We might say that the propagating signal fields in the FR-4 medium leave “**eddy currents**” in their wake as they carry information between a transmitter and a receiver. This model of **current density** flow in an adjacent conductor preserves causality.

Rough Surfaces: Real conductor surfaces are not perfectly flat. Copper surfaces are intentionally manufactured to be rough in order to make them adhere to a dielectric propagating medium in a laminate stackup under temperature and pressure; a peel test is typically used to determine the quality of the adherence. Figure 8 shows the degree of surface roughness in four different scanning electron microscope magnifications of a six layer high profile layer printed circuit board manufactured for this research. Etched microstrips (top and bottom), embedded fiberglass bundles, a resin solder mask, and several impurities can be seen in the photographs.

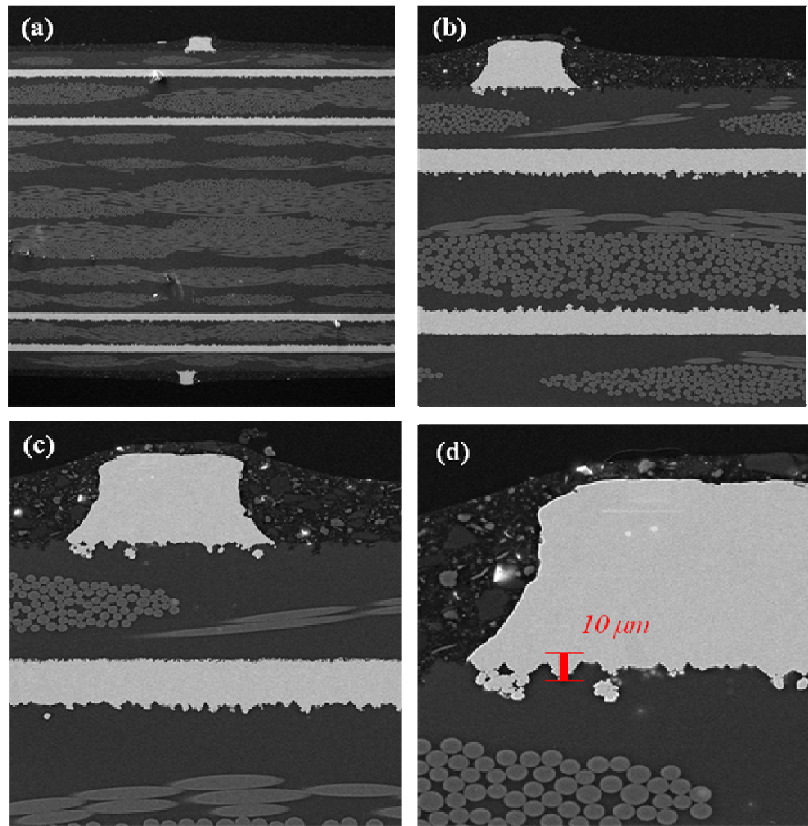


Figure 8. Four scanning electron microphotographs of a six layer, high profile, rough copper, FR-4 printed circuit board with embedded fiberglass bundles, a resin solder mask, and several impurities. Photo (d) shows a **10 μm** bar in red for reference.

Because the **magnetic** and **electric** field intensity propagates into copper relative to the skin depth, δ , we note that

$$\delta(\omega) = \begin{cases} 2.1 \mu m & \text{at } 1 \text{ GHz} \\ 0.66 \mu m & \text{at } 10 \text{ GHz} \\ 0.21 \mu m & \text{at } 100 \text{ GHz} \end{cases} \quad (3)$$

Thus, the skin depth at 1 GHz is comparable to some of the surface irregularities on the underside of the copper trace while at 100 GHz it is much smaller as is shown in detail below.

Rough Surface Manufacturing Process: A typical copper foil manufacturing process is shown in figure 9.

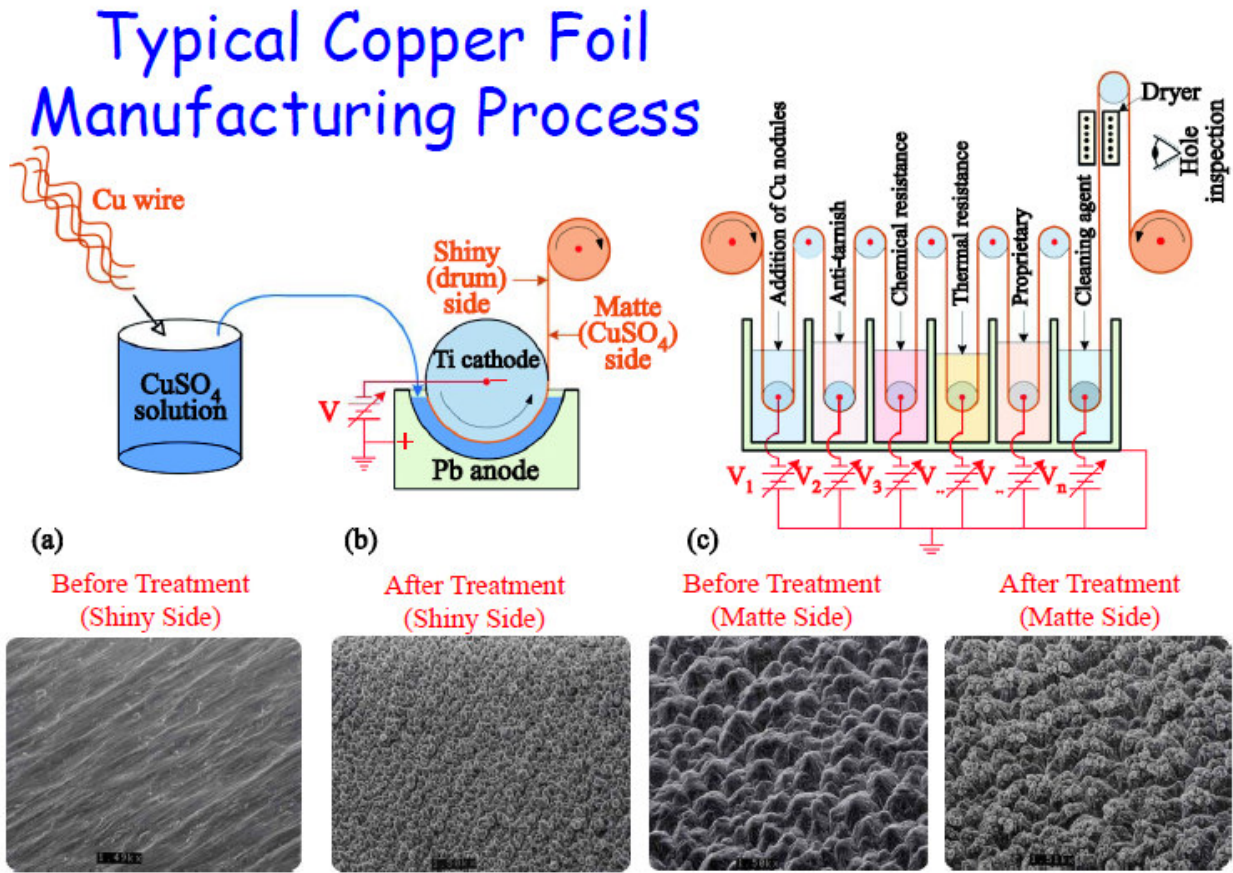
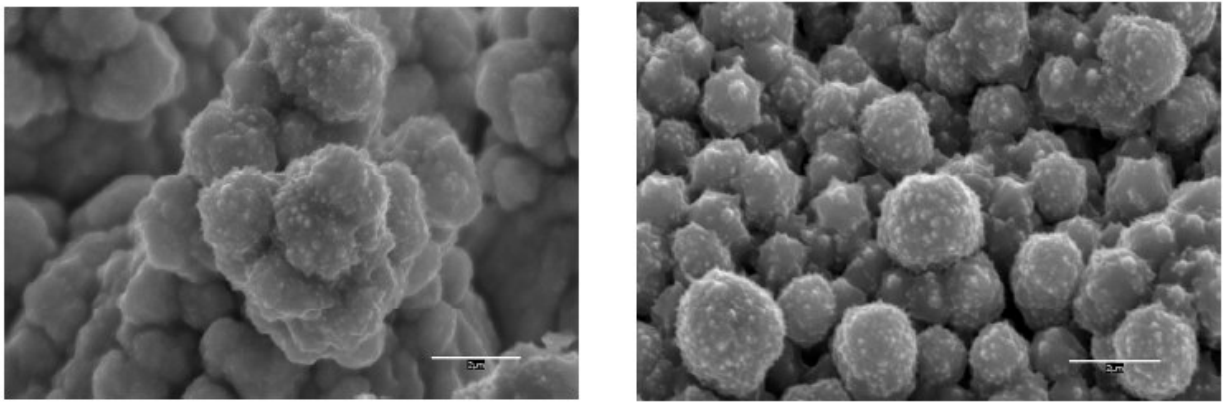


Figure 9. a. Purification of copper in a CuSO₄ solution. b. electrodeposition of copper onto a rotating titanium drum. c. Subsequent chemical processes that add copper nodules, protect the copper surface from tarnishing, make the surface resistant to Br contained in typical FR-4, and other proprietary surface treatments. Bottom photographs are SEM images of the drum side and CuSO₄ side of the copper foil surface before and after chemical treatment.

The process permits the custom manufacture of very smooth or very rough copper surfaces for different applications. However, the after treatment copper foils that are used in PCBs typically have a nodule texture as shown in figures 10 and 11.



High Profile texture

Low Profile texture

Figure 10. Scanning electron microscope photographs taken at a 32° angle of incidence for a high profile and low profile structure. The white bars in the lower right corner of each photo are 2 μm long.

In figure 10 we see the high profile samples resemble copper nodule pyramid structures arranged in a nominal hexagonal pattern on a matte finish surface. By comparison, the low profile samples appear to be made up of similar size copper nodules randomly scattered on a flat plane; the nodules vary in radius but the average size is about 1 μm in diameter.

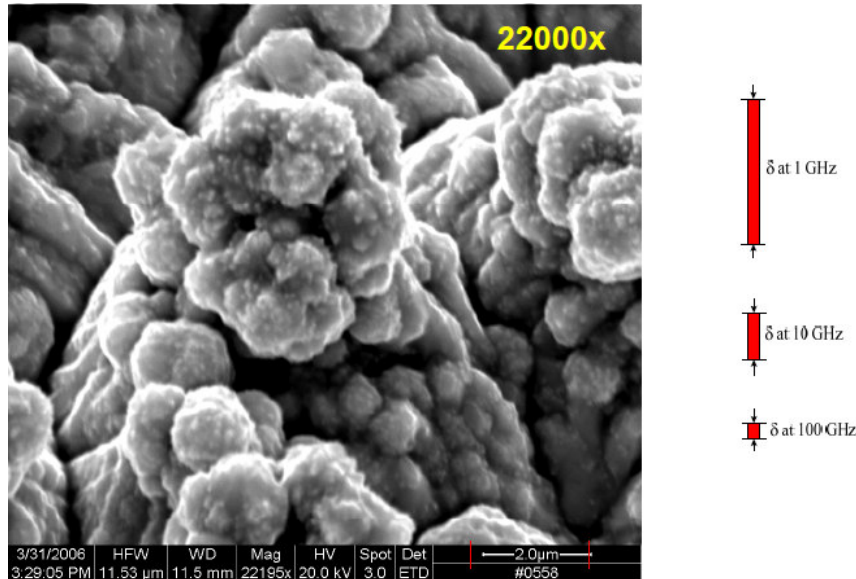


Figure 11. Scanning electron microphotograph of another high profile surface relative to skin depth δ at 1 GHz, 10 GHz, and 100 GHz.

From figure 11 we can see that the anchor nodules that appear as a pyramid stack have a number of nooks and crannies that can grasp heated FR-4 resin under pressure to provide good physical

adherence. Other features of the stackup are that the nodules themselves are possibly made up of very small kernels that form together in clumps like “snowballs.” Many former studies of voids in the pyramidal stack-up, average density of the surface copper compared to solid copper, and electrical resistivity of the surface material, are consistent with this construction. Clearly, it will be difficult, if not impossible, for any “simple” 2 dimensional analysis or model to properly represent the complex nature of the surface.

In addition, we have made Auger measurements to determine the chemical composition of the surface “snowballs” and have found an exponential change from brass (CuZn) to pure copper with a depth of about 200 nm and small concentrations of C, O, Si and Ni. These elements are intentionally added in the manufacturing process (Figure 9); Zn to protect the copper surface from oxidation, Si to protect the Zn from Br in the FR-4, and other subtle negative chemical effects. The electrical importance of the additions is that they cause a snowball surface film with lower conductivity and isolate the surface charge on individual snowballs from one another.

Measurements of the physical extent of the snowball pyramids have also been made with the help of a laser profilometer as shown in figure 12.

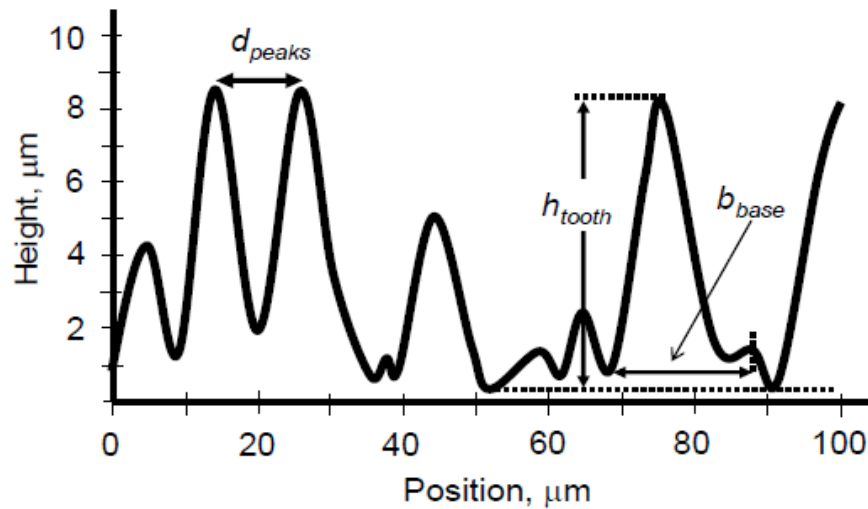


Figure 12. Laser profilometer measurement of a high profile copper surface used in insertion loss measurements. Many similar scans led to an RMS profile of stack-ups with a tooth height of $9.4 \mu\text{m}$ and a base width of $5.8 \mu\text{m}$.

If anything, the results of figure 12 show us the limitations of using a laser profilometer to determine the structure of a 3-D stack-up of copper material like that shown in figures 10 and 11. Because the size of the laser probe has a radius of about $2 \mu\text{m}$, the tool is relatively blunt and shows only large features from an overhead perspective to a vertical resolution of $0.2 \mu\text{m}$. The stylus of a diamond tip profilometer typically has an even more blunt radius of up to $10 \mu\text{m}$.

Non-uniform snowball model: To describe the power loss more precisely and analytically, we have constructed a model of a snowball stack-up in which spheres of various radii, located at various distances below a flat plane act to absorb and scatter the electromagnetic waves that propagate under the rough surface of a transmission line as shown in figure 13.

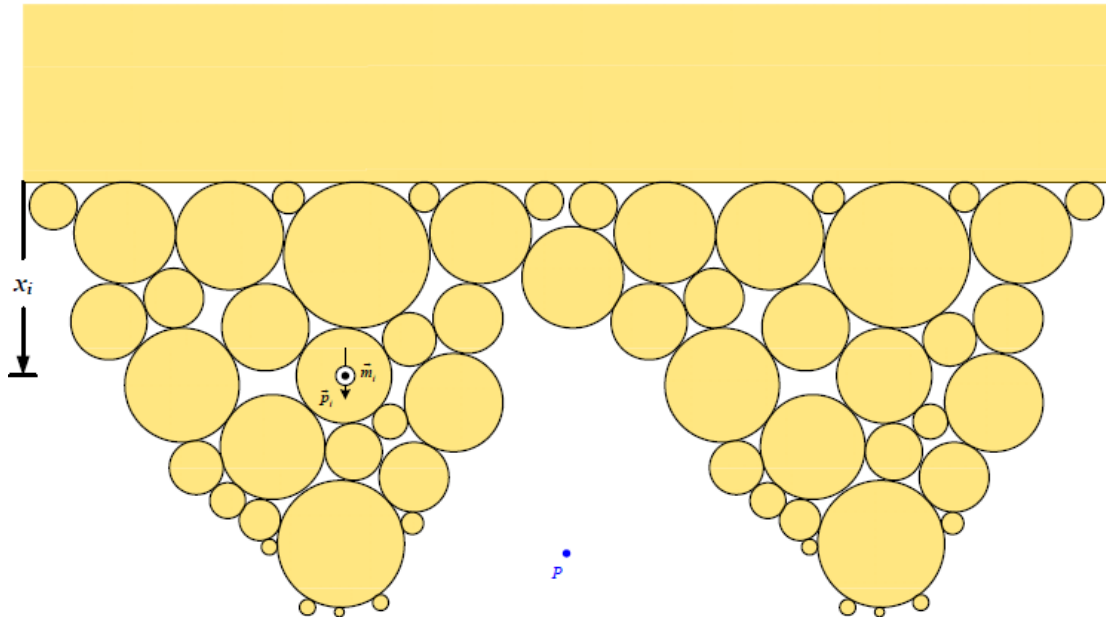


Figure 13. Cross-Section of a stack-up of a number of non-uniform copper snowballs located distance x_i below a flat surface to form a pyramid.

When the i^{th} copper sphere experiences an external **electric** and **magnetic** field intensity of a propagating TEM mode, it yields an **electric dipole moment**, \vec{p}_i , and a **magnetic dipole moment**, \vec{m}_i . The field at point P due to the constructive interference of the propagating fields and the scattering and absorption of the i^{th} copper sphere can be calculated by a partial wave analysis as was done^x in *The Foundations of Signal Integrity* to yield an effective cross-section for scattering and for absorption. If the position of each snowball was known, it would be possible, in principle, to calculate the field intensities at point P due to all of the spheres on the surface and to evaluate the amount of power that is lost from the propagating TEM fields due to the rough surface. Such an exact calculation is not possible so many approximations have been made in approximating the fields at point P . The Born approximation technique has been employed to make the analysis with second order effects neglected. The most important of these approximations is listed below. Neglect of the:

- Quadrupole and higher multipole moments in absorption and scattering.
- Image fields due to the nearby conducting plane.
- Screening fields due to nearest neighbor scattered fields.
- Multiple scattering from 2 or more snowballs.
- Bragg scattering from a periodic structures of snowballs.
- Surface alloy on each snowball.

All of these secondary effects have been approximated and found to be less than 6% of the 1st order Born approximation components^{ix}. The small amount of scattered and absorbed power due to snowballs on the ground plane are included in the number under the trace. For comparison to the measured power losses, we have further assumed that the collection of non-uniform sphere radii can be approximated by using n copies of the average uniform sphere; this assumption is somewhat self compensating in a 1st order approximation.

Uniform snowball model: Having little information about the distribution of snowball radii, the uniform average size has been chosen as a first approximation to see how well the power loss calculation works. As we have observed, the pyramid stack-ups occur in a more or less hexagonal form on the conductor surface. Since this is consistent with a hexagonal close packing for copper atoms on a surface and since the hexagonal geometry fills a flat area completely, we choose this structure for our analysis as shown in figure 14.

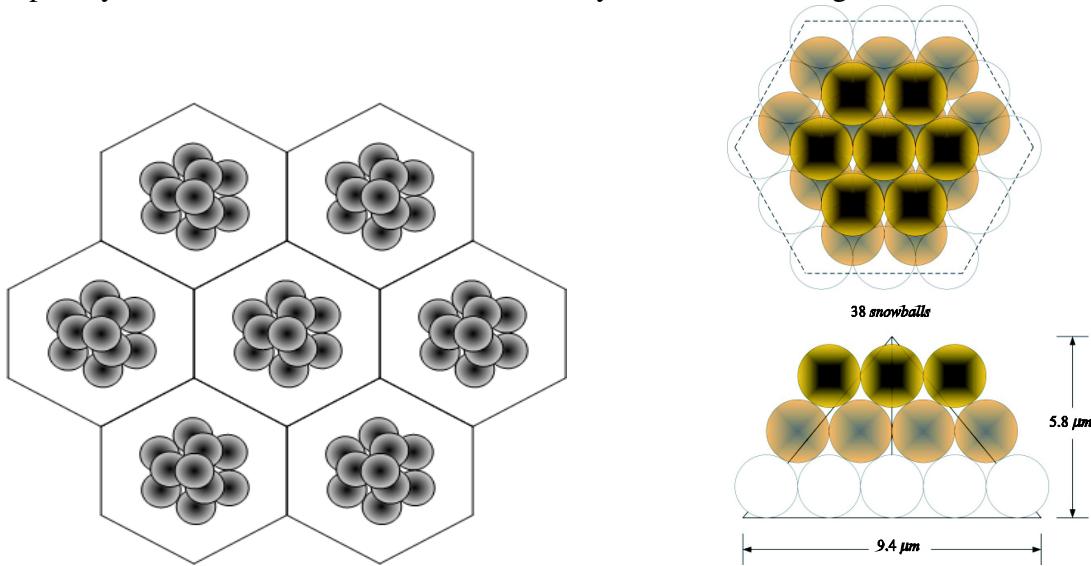


Figure 14. Left- Eleven 1 μm radius snowballs stacked into three layers on hexagonal cells with a height of about 5.8 μm . Right- Thirty Eight 1 μm radius snowballs stacked into three layers on hexagonal cells. Both schemes have a base dimension of 9.4 μm .

The hexagonal geometry choice has no bearing on the final power loss calculation but it gives us a basis to find the lower and upper limits for average size snowballs that fill the area and look something like the SEM photographs in figure 10 and 11. We can see from figure 14 that three levels of snowballs of radius are required to make a height of about 5.8 μm , that 11 spheres per hexagonal cell is too few to fill the area, and that 38 spheres per hexagonal cell is too many to form a pyramid like that observed in figures 10 and 11. Thus, in our analysis routines for the power lost, we would expect a number of uniform snowballs somewhere between these lower and upper limits. A similar process can be used to find lower and upper limits for smaller radii spheres.

First Principles Power Loss: To evaluate the power loss for an interconnect we employ the Born Approximation technique in which a sequence of perturbations of higher order are calculated for propagating electromagnetic fields. In principle, the technique would require an

infinite number of calculations but we can estimate the influence of each perturbation to find the percentage change. When the perturbation change is comparable to other neglected effects the process is terminated and each contribution evaluated. In the process the dielectric losses are considered independently from the losses due to conductor losses. We begin with the 0^{th} order Born approximation as shown in figure 15.

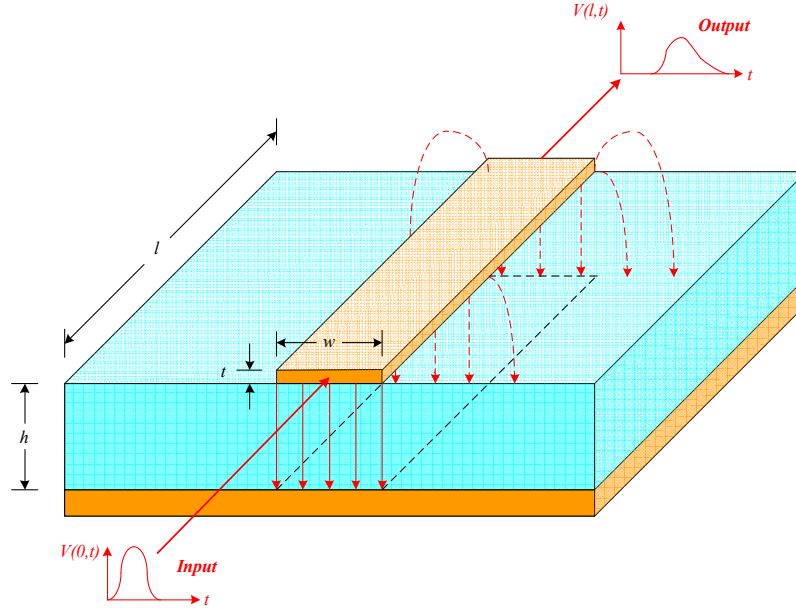


Figure 15. 0^{th} order Born approximation for the \vec{E} fields associated with a lumped signal as it propagates in a microstrip transmission line. The dielectric medium is assumed to be perfectly homogeneous and the conductors are assumed to be perfectly flat.

In the 0^{th} order Born approximation the **electric field intensity** caused by a signal pulse is taken to be in the x -direction, and the **magnetic field intensity** is taken to be in the y -direction as they propagate in the z -direction. The 1^{st} order Born approximation is then the absorption and scattering that occurs when a single snowball is placed in the path of propagation as shown in figure 16.

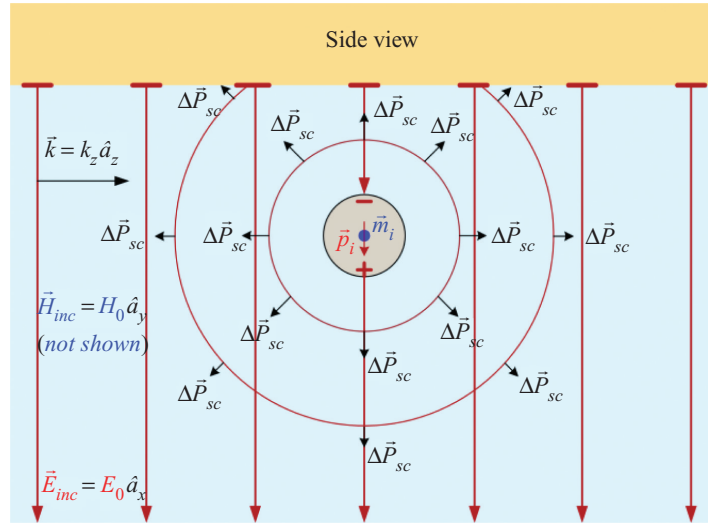


Figure 16. Side view of a microstrip transmission line with a spherical conductor perturbation as an incident TEM electromagnetic wave propagates in the z -direction. The power scattered from the conducting sphere is shown as an outgoing wave. The power absorbed by the sphere would be represented by an incoming wave (not shown in this graphic to preserve clarity).

In the 1^{st} Born approximation we take incident plane waves to be of the form

$$\begin{aligned}\vec{E}_{inc}(\vec{x},t) &= \vec{E}_0 e^{j(\vec{k} \cdot \vec{x} - \omega t)} \hat{a}_x \quad \text{with } \vec{k} = k_{die} \hat{a}_z \\ \vec{H}_{inc}(\vec{x},t) &= \vec{H}_0 e^{j(\vec{k} \cdot \vec{x} - \omega t)} \hat{a}_y\end{aligned}\quad (4)$$

to calculate the average scattered power, $\langle \Delta P_{sc} \rangle$, and the average absorbed power, $\langle \Delta P_{abs} \rangle$, in terms of the average incident power density $\vec{\mathcal{P}}_{inc} = (1/2) \operatorname{Re} [\vec{E}_{inc} \times \vec{H}_{inc}]$ in terms of a scattering cross section:

$$\begin{aligned}\langle \Delta P_{absorbed} \rangle / |\vec{\mathcal{P}}_{inc}| &= \sigma_{absorbed} \\ \langle \Delta P_{scattered} \rangle / |\vec{\mathcal{P}}_{inc}| &= \sigma_{scattered}\end{aligned}\quad (5)$$

These quantities are found by solving Maxwell's equations in spherical coordinates and applying tangential boundary conditions for a sphere required by surface impedance as discussed following figure 6. The resulting fields that penetrate the good conducting sphere are shown in figure 17.

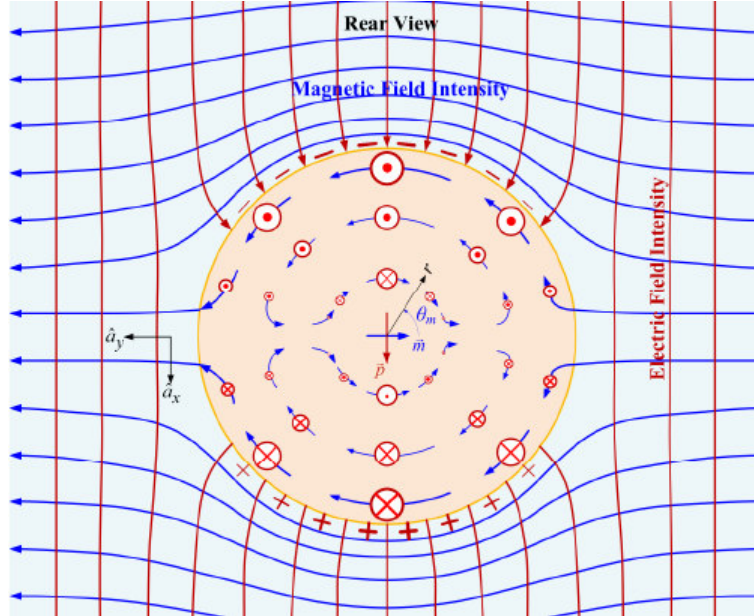


Figure 17. Rear view of the analytic solution to Maxwell's equations for a propagating incident electric and magnetic field intensity wave as it interacts with a good conducting sphere.

Cross sections for the 1^{st} Born approximation have been found^x with the help of partial wave analysis that interprets incoming wave power as absorbed and outgoing wave power as scattered under the boundary condition required for tangential fields with a spherical surface impedance. Neglecting quadrupole and higher multipole terms the analysis gives:

$$\begin{aligned}\sigma_{\text{absorbed}}(\omega) &\approx 3\pi k_2 a_i^2 \delta / \left[1 + \frac{\delta}{a_i} + \frac{\delta^2}{2a_i^2} \right] \\ \sigma_{\text{scattered}}(\omega) &\approx \frac{10\pi}{3} k_2^4 a_i^6 \left[1 + \frac{2}{5} \left(\frac{\delta}{a_i} \right) \right]\end{aligned}\quad (6)$$

We can observe from equations 6 that for high frequencies where the skin depth, $\delta(\omega)$, is small compared to a snow-ball radius, a_i , the **cross section for scattering** is the same as the classic power radiated by Rayleigh scattering^{xi} ($\omega^4 a_i^6$). At frequencies where the skin depth, $\delta(\omega)$, is small compared to a snow-ball radius, a_i , the **cross section for absorption** behaves as ($3\pi k_2 a_i^2 \delta$). The frequency dependence of these scattering cross sections are shown in figure 18.

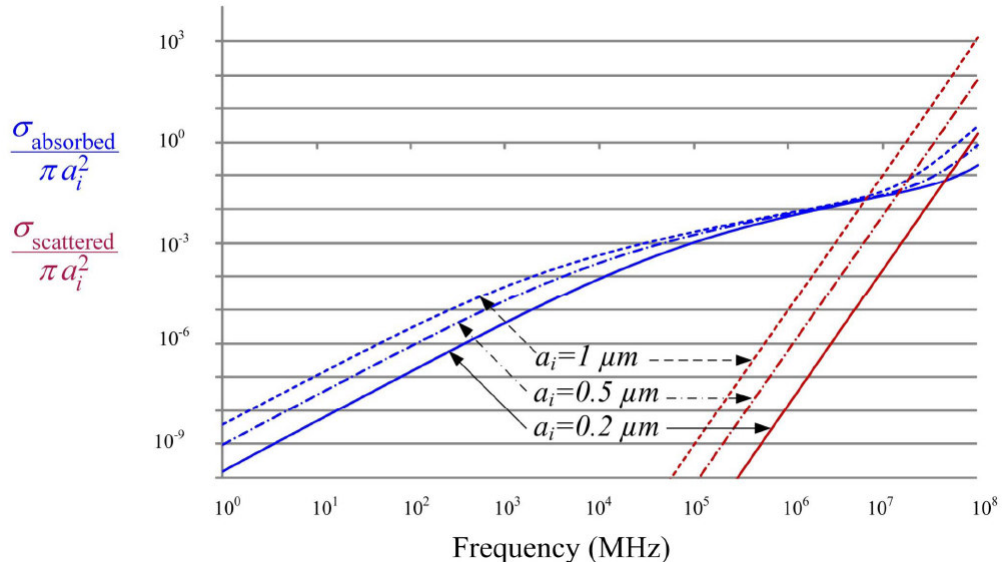


Figure 18. Values of the **absorbed** and **scattered** cross sections of a copper sphere (relative to their geometric cross section) as a function of frequency.

From figure 18 we can see that for conducting spheres of radii $a_i=0.2 \mu m$, $a_i=0.5 \mu m$, or $a_i=1.0 \mu m$ and frequencies below about 10 THz the cross section for absorption is larger than the cross section for scattering and below 100 GHz, we can ignore the scattered power.

Application to multiple snowballs: As we noted in figure 13, we can model the rough surface pyramidal stack ups of copper “snowballs” to first approximation as a collection of N_i spheres, each of radius a_i . Using the **absorption cross section** for high frequencies ($3\pi k_2 a_i^2 \delta$) we can then compute the maximum power absorbed by the stack up of the spheres as:

$$\Delta P_{\text{smooth}} + \sum_{i=1}^j N_i \Delta P_i \approx \frac{1}{4} \mu_c \omega \delta |\mathbf{H}_0|^2 A_{\text{hex}} + \sum_{i=1}^j N_i \frac{1}{2} |\mathbf{E}_0 \times \mathbf{H}_0| 3\pi k_2 a_i^2 \delta \quad (7)$$

so

$$\left[P_{\text{rough}} / P_{\text{smooth}} \right]_{\text{Maximum}} \approx 1 + \frac{3}{2} \sum_{i=1}^j N_i 4\pi a_i^2 / A_{\text{hex}} \quad (8)$$

Equation 8 is important because it shows that the maximum power lost at high frequencies where the skin depth, $\delta(\omega)$, is small compared to a snow-ball radius, a_i , is unlimited, depending only on the area of all of the “snowballs” or “anchor nodules” on a hexagonal area relative to the flat copper surface area upon which they sit. The power lost in this model is independent of RMS deviation of the snowball stack up height or the RMS surface roughness!

Comparison with measured power loss: Using equations 6 we can calculate the power loss for a stack up of different size snowballs on a flat surface as a function of frequency as:

$$\frac{P_{\text{rough}}}{P_{\text{smooth}}} \approx 1 + \frac{3}{2} \sum_{i=1}^j \left(\frac{N_i 4\pi a_i^2}{A_{\text{hex}}} \right) \left/ \left[1 + \frac{\delta}{a_i} + \frac{\delta^2}{2a_i^2} \right] \right. \quad (9)$$

Design engineers at Intel call this the special form of the Huray equation for a flat surface (non-Matte finish) substrate; it replaces the Hammerstad equation (1) as a predictor of the conductor power loss into a textured surface.

Measurements of surface roughness copper microstrip and striplines of various lengths have been made with different dielectric media (FR-4, Isola, Rogers, Nelco) to test the validity of the Huray equation. VNA insertion loss measurements for a 7 inch high profile trace are shown in figure 19 as a function of frequency up to 50 GHz:

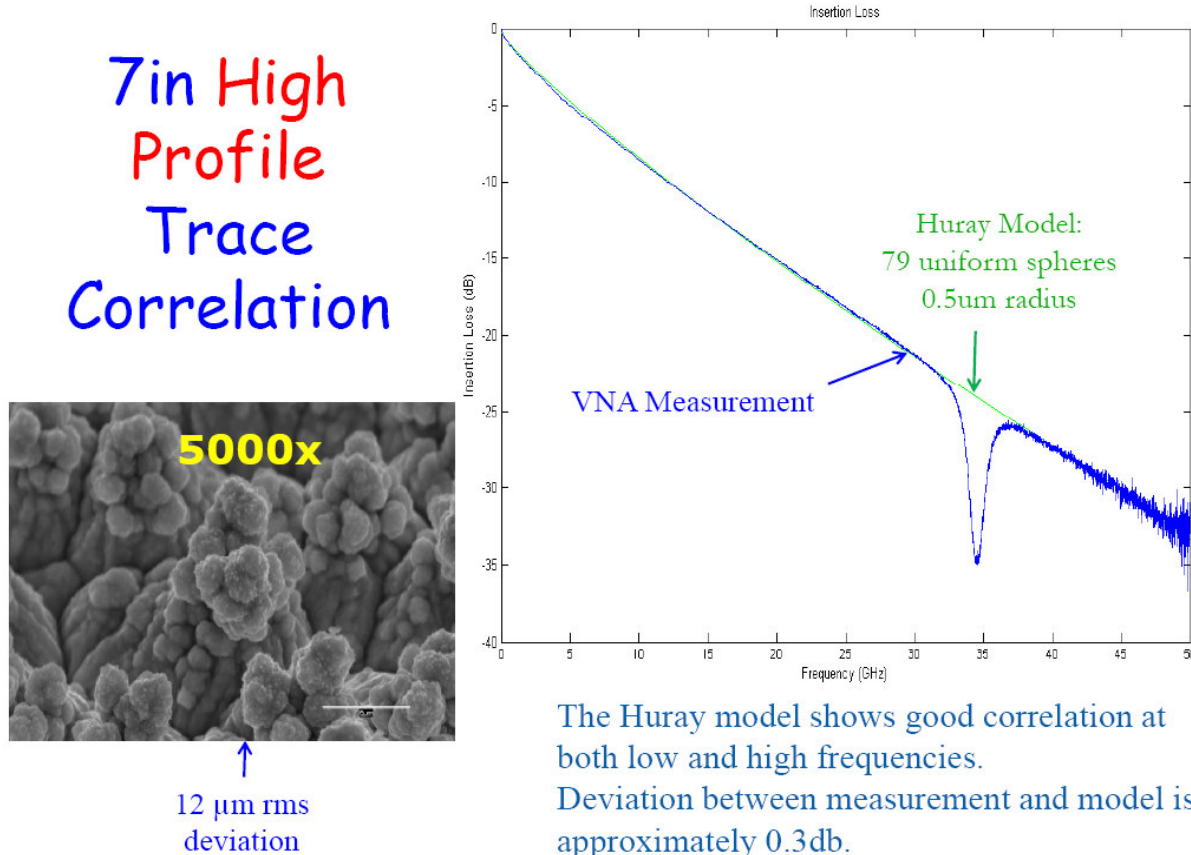


Figure 19. Comparison of VNA insertion loss measurements for a 7 inch **high profile** ($12 \mu\text{m}$ rms deviation) microstrip and the predictions of the **Huray model** with 79 uniform spheres of radius $0.5 \mu\text{m}$ as a function of frequency.

For a contrasting comparison we show in figure 20 the results of a **low profile** surface roughness for a 7 inch microstrip.

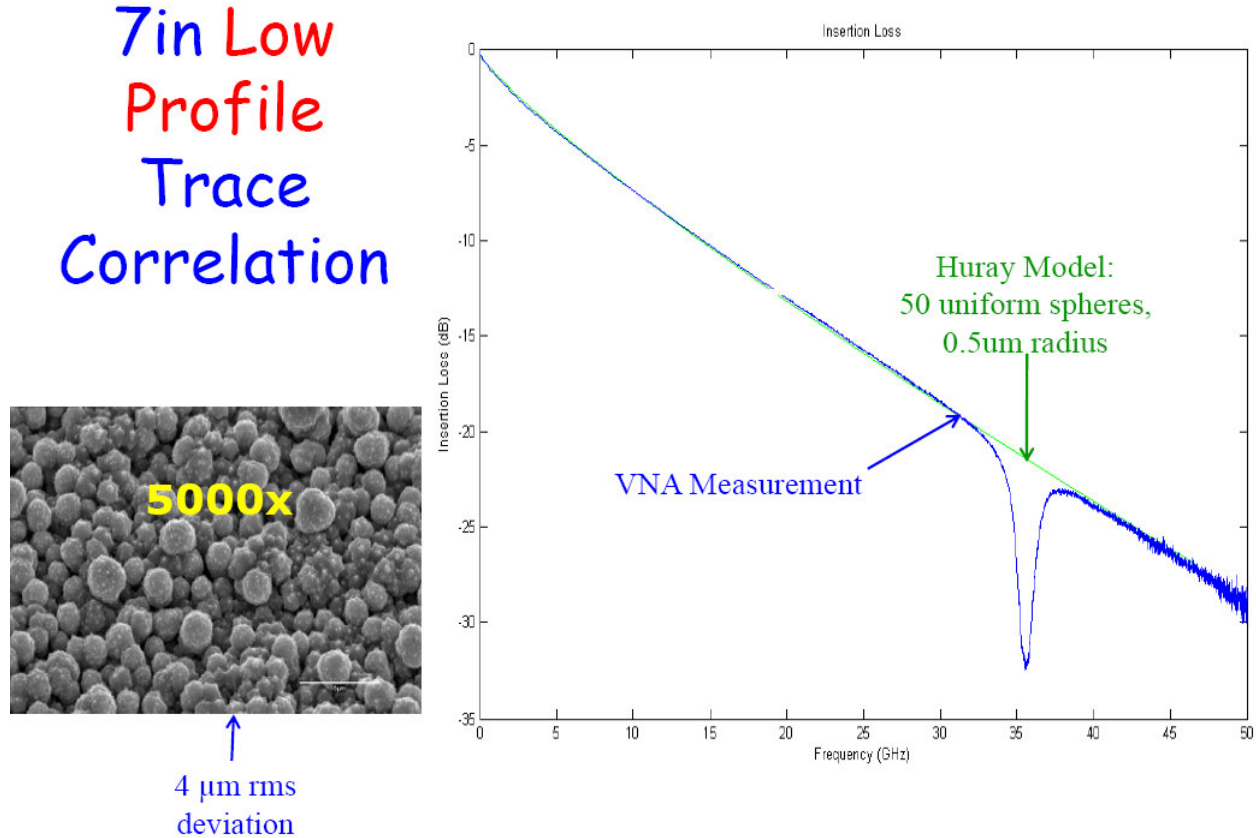
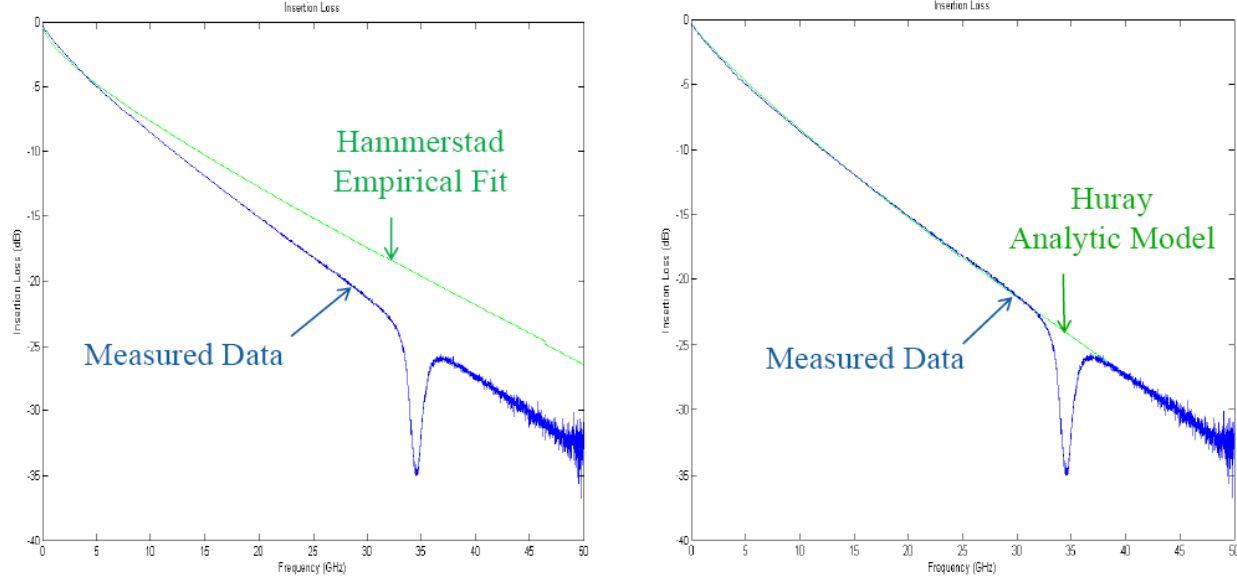


Figure 20. Comparison of VNA insertion loss measurements for a 7 inch **low profile** ($4 \mu\text{m}$ rms deviation) microstrip and the predictions of the **Huray model** with 50 uniform spheres of uniform spheres of radius $0.5 \mu\text{m}$ as a function of frequency.

We can see from these two comparisons that the insertion power loss for both high and low profile surface roughness is large and that the **Huray model** accurately predicts the loss with frequency up to 50 GHz without any reference to RMS deviation!

2nd Order Born Approximations^{xii}: The Huray model profits from several instances of serendipity for frequencies below 100 GHz: In a partial wave analysis the absorbed power calculated right at the nodule's surface gives the same power as the asymptotic answer. The absorption cross section is very small compared to geometric^{xiii} so that we can sum over groups of nodules without regard for their surroundings. The scattered power can be neglected and thus the asymptotic partial wave analysis does not require secondary fields scattered from neighboring nodules; screening by neighboring nodules is small enough to ignore to first order. The low conductivity of the nodule surface electrically isolates them from one another. The influence of surface coating on power loss is small compared to the loss due to the remaining copper. Quadrupole and higher multipole moments produce less than 1% of the power loss due to dipole moments. Image dipoles caused by a nearby smooth conducting plane *lowers* the total loss of an isolated snowball that absorbs and scatters.

Conclusions: The relative power loss for a rough surface constructed by adding anchor nodules to a flat copper foil can be accurately calculated using equation 9 with a set of uniform copper absorbing spheres of average radius equal to that of the observed “snowballs” in a pyramidal stack up. By comparison, the failure of the Hammerstad empirical fit to describe this loss is shown in figure 21.



Empirical Hammerstad fit of measurements based on 1948 Morgan 2-D surface model.

First principles Huray analytic absorption model based on observed surface texture of snowball stack-ups.

Figure 21. VNA measurements of insertion loss for a 7 inch long, high profile roughened microstrip with RMS deviation of $12 \mu\text{m}$ compared to: Left graph: An empirical Hammerstad fit that is based on the 1948 Morgan 2-D surface model that depends on the RMS surface roughness and Right graph: A first principles analytic absorption and scattering Huray model that depends only on the relative area of the extra “snowballs” and a dipole scattering dependence.

It is probably serendipity that permits a compensation of pre-treated copper foils as flat even if the after-treatment nodules are deposited on a *non-flat* Matte surface. If we correct the relative power loss equation 9 for this additional area we should replace the term 1 with the ratio of the average Matte area perturbation to a flat hexagonal area:

$$\frac{P_{rough}}{P_{smooth}} \approx \frac{A_{Matte}}{A_{hex}} + \frac{3}{2} \sum_{i=1}^j \left(\frac{N_i 4\pi a_i^2}{A_{hex}} \right) \left/ \left[1 + \frac{\delta}{a_i} + \frac{\delta^2}{2a_i^2} \right] \right. \quad (10)$$

This is the general form of the Huray equation (including a *non-flat* Matte finish) and it should be valid for a large category of surface textures and for frequencies up to 100 GHz. It replaces the Hammerstad equation (1) as a predictor of the conductor power loss into a textured surface.

ⁱ S.P. Morgan Jr., “Effect of Surface Roughness on Eddy Current Losses at Microwave Frequencies,” *Journal of Applied Physics*, Vol. 20, p. 352-362, April, 1949.

ⁱⁱ E. O. Hammerstad and F. Bekkadal, *Microstrip Handbook*, Trondheim, Norway: Univ. Trondheim, 1975, pp. 4-8.

ⁱⁱⁱ E. O. Hammerstad and Ø. Jensen, “Accurate Models for Microstrip Computer Aided Design”, IEEE MTT-S Int. Microwave Symp. Dig., pp 407-409, May 1980.

^{iv} Steven Hall and Howard Heck, *Advanced Signal Integrity for High Speed Digital Designs*, John Wiley & Sons, Hoboken, NJ (2009) p. 242.

^v P.G. Huray, Y. Chen, and R. Mellitz, “Physics of Scattering from Inclusions in FR-4 and Rough Trace Surfaces,” Intel USC Dedication Poster, Feb. 25, 2005.

^{vi} P.G. Huray, S.G. Pytel, R.I. Mellitz, S.H. Hall, “Dispersion Effects from Induced Dipoles”, 10th Workshop on Signal Propagation on Interconnects, Berlin Germany, May 9–12, 2006.

^{vii} P. G. Huray, S. Hall, S. G. Pytel, F. Oluwafemi, R. Mellitz, D. Hua, and P. Ye, “Fundamentals of a 3-D “Snowball” Model for Surface Roughness Power Losses”, IEEE conference on Signals and Propagation on Interconnects, May 14, 2007, Genoa, Italy.

^{viii} An apparent resonance absorption peak is observed in the measured data from the sample prepared by Merrick at about 35 GHz. Because this paper focuses on the losses due to surface roughness we refer the reader to Huray, *The Foundations of Signal Integrity*, John Wiley & Sons, Hoboken, NJ (2010) pp. 198-215 for a discussion about dielectric losses.

^{ix} Jon Mathews and R.L. Walker, *Mathematical Methods of Physics*, W. A. Benjamin, Inc., New York (1965) p.289

^x Huray, Ibid, p. 264.

^{xi} Lord Rayleigh, Philos. Mag. 41 (1871): 107, 274.

^{xii} Huray, Ibid, *Chapter 7: Advanced Signal Integrity*.

^{xiii} We are grateful for private communications with John David Jackson, author of *Classical Electrodynamics*, 3rd Edition, John Wiley & Sons (1999), Hoboken, NJ for a discussion of partial wave analysis techniques.